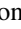



Droplet impact on rotating surfaces: The effect of centrifugal force and wettability on spreading dynamics

Dongdong Liu *, Hongdong Yin, Zeyu Wu, and Xiang Luo
School of Energy and Power Engineering, Beihang University, Beijing, China

 (Received 17 April 2024; accepted 31 July 2024; published 19 August 2024)

Droplet impact on rotating surfaces experiences the tangential shear force from the rotating surface, generating a centrifugal force that either enhances the spreading or destabilizes the expanding lamella. In this study, we experimentally characterize the impact of a water droplet on rotating surfaces with various wettabilities, and theoretically analyze the observed impacting dynamics, including the enhanced spreading and the transition to the destabilization of the expanding lamella. Liquids with a wide range of viscosity are tested to explore the effect of liquid viscosity on the impacting dynamics. We propose a simplified approach to predict the tangential velocity induced by the surface's tangential shear force, and validate the predicted velocity by flow field measurement. We further deduce a quantitative description for the maximum spreading factor in the spreading regime, and derive the critical condition for the destabilization of the lamella for a water droplet. Good agreements are found between the predicted values and the measured ones for the impact on the rotating surfaces with various wettabilities.

DOI: [10.1103/PhysRevFluids.9.083605](https://doi.org/10.1103/PhysRevFluids.9.083605)

I. INTRODUCTION

The interactions between the droplet and the interface, due to the rich phenomena in short duration, are widely applied in various industrial applications, including ink jet printing, spray cooling, and agricultural irrigation [1–3]. Diverse dynamics of the droplets during the impact on various interfaces [4–7] attract great interests to observe, characterize, and further predict the droplet's behavior.

Upon impact, the droplet deforms under the reacting force from the surface, possibly trapping a small volume of air underneath, and ejects a thin liquid sheet, entitled as the lamella, from the deformed liquid body [8]. This radially expanding lamella, resisted by the viscous force and the capillary force, either reaches its maximum spreading diameter, or induces liquid disintegration at its advancing front. The former behavior is referred to as spreading, while the latter one as splashing. These two typical behaviors of the impacting droplet are affected by various factors, including the droplet's physical property [9–11], surface wettability [1,12–14], surface morphology [15–18], and ambient condition [19]. Tuning one of these factors may induce the transition between spreading and splashing [20], or the emergence of new impacting behaviors [21,22]. With a set combination of droplet and surface, the transition of the droplet's behavior from spreading to splashing is normally triggered by the increase of the impacting velocity [23].

To capture the key characteristics of these two behaviors, i.e., the maximum deformation of the spreading droplet and the splashing threshold, numerous models, either from the perspective of energy conservation [24,25] or from the view of force balance [26], were proposed to reveal the underlying physical mechanism. Although a universal model is favorable, the droplets' properties

*Contact author: ddliu@buaa.edu.cn

and surfaces' conditions were found to significantly affect the droplets' impacting dynamics. Therefore, each model was proposed based on the specific impacting condition. For instance, the maximum spreading factor β_{\max} of a water droplet on a superhydrophobic surface was found to be scaled only by the impacting Weber number We . For a droplet with high viscosity, β_{\max} was found to be simply associated with the Reynolds number Re due to the significant role of the viscous dissipation. Accurate quantifying of the energy budget for an impacting droplet may be a promising approach in tendering a universal scaling law of the maximum spreading factor β_{\max} for various impacting conditions. However, the variation of the impacting condition may change the boundary conditions of the impact and reshape the energy equation. For instance, the artificially added external excitation on the interface, including the acoustic wave [27], the surface's motion [21,28,29], and vibration [30,31], may significantly change the dynamics of the boundary layer in the advancing lamella during spreading, and generate discrepancies between the measured values of β_{\max} and the predicted ones from the model derived for impacting on the static surface.

For the transition of the droplet's behavior from spreading to splashing, the aerodynamic force from the surrounding air has been found to play a vital role in triggering the splashing [20]. The escaping air flow underneath the expanding lamella either destabilizes the liquid film [32] or consistently lifts the lamella up in the air until its breakup [8]. Such splashing mechanisms were found to well describe the transition for the impact occurring on a smooth and flat surface with various wettability. However, for impact on rough, soft, or inclined surfaces, the complex droplet-interface interaction complicates the spreading-splashing transition, resulting in a newly emerged mechanism and critical parameter of splashing [21,33–35].

For the interaction between the droplet and the moving interface, it originates from the interaction between the droplet and the moving surfaces appearing in engineering applications. These scenarios include the rain droplet impacting on the moving train or the rotating parts of the aeroengine or wind turbine generator [36,37]. The applied surface motion induces additional shear force between the droplet and the target surface, resulting in the emergence of new spreading and retracting dynamics [38]. For the impact far away from the rotating center, the tangential shear force from the surface could be considered as constant during impact, generating an asymmetric spreading by applied stretching force in the tangential direction [29,39]. In contrast, for the impact right on the rotating center, shear force is symmetric in the tangential direction and develops with the spreading radius, resulting in the dominant effect of the centrifugal force on the spreading dynamics. For a rough superhydrophobic surface, the centrifugal force stretches the spreading droplet and generates a hole in the middle of the droplet, resulting in a rapid rebound [40]. However, the effect of the surface's wettability on the droplet's dynamics for the impact right on the center of the rotating surface is not fully understood. The underlying mechanism, i.e., how the shear force and the centrifugal force from the rotating surface change the spreading dynamics of the impacting droplet, is still missing.

In this study, we intend to give a full picture of the droplet's spreading dynamics when impacting on the center of a rotating surface qualitatively and quantitatively. We explore the droplets' behaviors for impacting right on the center of the rotating surfaces with various wettabilities and a wide range of liquid viscosities. We use high-speed imaging to observe the impact behavior and characterize the behavior for wide ranges of experimental parameters, including the impacting velocity V_0 , rotating speed ω_0 of the surfaces, liquid viscosity, and the surface wettability. We propose a model to predict the maximum spreading diameter in the spreading regime for all liquids and the transition between the impacting behaviors for water.

II. EXPERIMENTAL SETUP

We use distilled water and water-glycerol mixtures as the working liquids. The water-glycerol mixtures with different weight ratios are prepared to obtain liquids with different viscosities. For the water droplet, its initial diameter D_0 is $2.8 \text{ mm} \pm 0.1 \text{ mm}$ or $3.5 \text{ mm} \pm 0.1 \text{ mm}$, while it is changed to $2.4 \text{ mm} \pm 0.1 \text{ mm}$ for a droplet of water-glycerol mixture due to the reduced surface tension. Droplets are generated by supplying a liquid through a flat tip needle and released from the

TABLE I. Physical properties of the liquids used in this study.

Liquid	Viscosity (mPa s)	Density (kg m^{-3})	Surface tension (mN m^{-1})
Water	1	1000	72.0
Water-glycerol mixture 1	5	1117	68.5
Water-glycerol mixture 2	10	1150	67.3
Water-glycerol mixture 3	50	1203	65.3
Water-glycerol mixture 4	100	1219	64.9

needle by gravity. We vary the releasing height of the droplet from 10 to 600 mm to obtain a velocity range between 0.3 m s^{-1} and 3.4 m s^{-1} . The resulting Weber number, defined as $We = \rho V_0^2 D_0 / \sigma$, varies from 5 to 560. Here, σ and ρ are the surface tension and density of the liquid at room temperature, respectively (Table I). By changing the viscosity of the liquid from 1 to 100 mPa s, the resulting Ohnesorge number, defined as $Oh = \mu / (\rho D_0 \sigma)^{1/2}$, ranges between 0.002 and 0.23 in this study. Here, μ is the viscosity of liquid.

The schematic of the experiment setup is shown in Fig. 1(a). We assemble the surface to a circular platform, which is directly attached to one end of the rotating shaft of a vertical motor to obtain a horizontal rotating surface. The rotating speed ω_0 of the motor is well controlled between 0 and 10 000 revolutions per minute (rpm), by a control unit. The resulting rotational Reynolds number $Re_\omega = \rho \omega_0 D_0^2 / \mu$ ranges from 0 to 13 000. In the experiment, we make sure the horizontal distance Δx between the center of the falling droplet and the center of the rotating surface is less than 10 pixels (1 pixel = $17 \mu\text{m}$) for all impacting cases, since we find the deviation of the maximum spreading factor between cases in this range is almost the same as those on a static surface. To measure the horizontal distance, we first identify the rotating center of the surface in the recording camera before measurement, and compare it with the center of the falling droplet. We exclude the cases with large horizontal deviation from the rotating center of the surface, i.e., $\Delta x > 170 \mu\text{m}$. To reduce the horizontal deviation for each impact, we place the needle in a long metallic tube to reduce the disturbances from the surrounding environment. For each impact, we repeat the experiment several times to ensure at least three qualified repetitions for data processing.

To explore the effect of surface wettability on the spreading dynamics, we prepare five surfaces with different materials, including glass, polymethylmethacrylate (PMMA), paraffin wax (PW), polished aluminum (Al) and silicon surface coated with nanoparticles (superhydrophobic surface, or SHBS). The static contact angle α_θ of a water droplet on the surfaces ranges from 12° to 165° (Table II), suggesting that the wetting properties of these surfaces range from hydrophilic

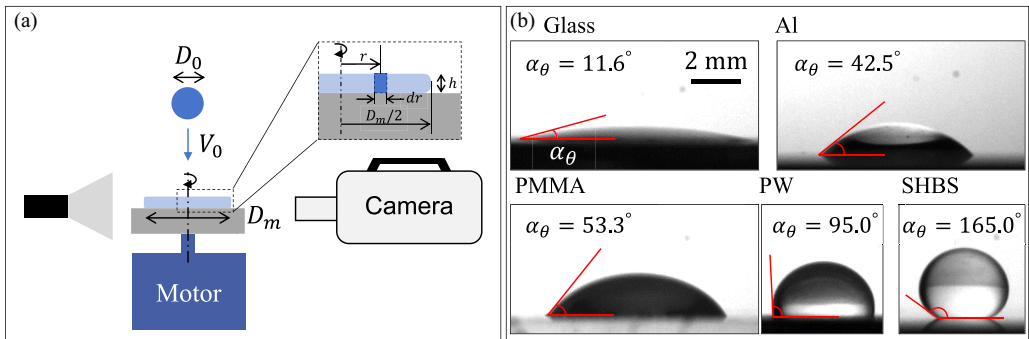


FIG. 1. (a) Schematic (not to scale) of the experiment setup for droplet impact on a rotating surface. Inset: schematic of the generated lamella at the maximum spreading diameter ($t = t_c$). (b) Sessile water droplets on the five tested surfaces of different materials. The static contact angle α_θ is measured from the image to indicate the surface's wettability.

TABLE II. Static contact angle α_θ and advancing contact angle α_a for a water droplet on the tested surfaces in this study.

Surfaces	Glass	Aluminum	PMMA	PW	SHBS
Static angle α_θ ($^\circ$)	12	43	53	95	165
Advancing angle α_a ($^\circ$)	58	88	92	132	180

to superhydrophobic [Fig. 1(b)]. The advancing contact angle α_a , ranging from 58° to 180° , is also measured for a prediction of the maximum spreading factor. The contact angle and the advancing contact angle of the water-glycerol mixture droplet on the PMMA surface are around 72° and 82° , respectively.

To visualize the flow field inside the droplet, silver-coated hollow glass particles with the size of $10\ \mu\text{m}$ and the same density of water are seeded into the droplet before impact. The seeding density of the particle is set around 0.006 particles per pixel (ppp). This seeding density is significantly below the critical seeding density, 0.17 ppp, over which image contrast would significantly decrease due to the loss of optical transmission in the seeded liquid [41]. A silver-coated mirror is assembled on top of the impacting surface, beside the needle, providing the angled top view of the spreading droplet. In the flow field measurement, we measure the flow field in the expanding lamella when the droplet is reaching the maximum spreading diameter. We first determine the droplet's expanding diameter and impacting center from the recording, and then decompose the measured velocity into two perpendicular directions, one in the radial direction and the other in the circumferential direction. The velocity in the circumferential direction is the tangential velocity of the spreading droplet on the rotating surface.

For each impact, we record the behavior of the droplet impact targeted on the center of the rotating surface using a high-speed camera (Nova S9, Photron). The images from both the angle view and the side view are recorded in the experiment for analysis. The frame rate of the camera is set to 20 000 fps. We use a lens (Micro-NIKKOR, 105 mm, f2.8) attached to an extension tube to record images with a pixel size of $17\ \mu\text{m}$. A light-emitting diode light source provides the illumination.

III. RESULT AND DISCUSSION

A. Characteristic behaviors of impacting droplets on rotating surfaces

To explore the impacting behaviors of droplets on rotating surfaces, we systematically vary the impacting velocity V_0 and rotating speed ω_0 of the surface, and record the impact behavior for different combinations of surface and liquid. We observe different spreading behaviors of the droplet, besides the typical spreading and splashing. In Fig. 2, we present five series of representative snapshots, showing the typical behaviors of the impacting water droplets on the static or rotating surfaces with different ω_0 on a PMMA or PW surface. For a water droplet impacting on a static PMMA surface, i.e., $\omega_0 = 0$ [Fig. 2(a)], the droplet deforms and generates a thin liquid film upon impact, which expands to its maximum spreading diameter $D = D_m$ at $t = t_c$. Here, $t = 0$ is denoted as the moment when the droplet appears to contact the surface. The liquid film can either keep the radial position at maximum diameter D_m or retract by capillarity, depending on the wettability of the surface.

In contrast, the impacting behavior of the water droplet changes on the rotating surface ($\omega_0 > 0$). At low rotating speed [$\omega_0 = 2000$ rpm, Fig. 2(b)], the impacting droplet spreads to D_m on the PMMA surface ($t = 3.75$ ms), retracts to a certain radius ($t = 15$ ms), and then spreads again until the liquid film becomes unstable ($t = 30$ ms). This impact behavior is denoted as *spreading retraction* in this study. It has to be noted that the droplet may deposit on the hydrophilic surface after impact when $\omega_0 \leq 1000$ rpm, a behavior denoted as *deposition*. At high rotating speed [$\omega_0 = 6000$ rpm, Fig. 2(c)], the generated lamella keeps spreading until the destabilization of liquid

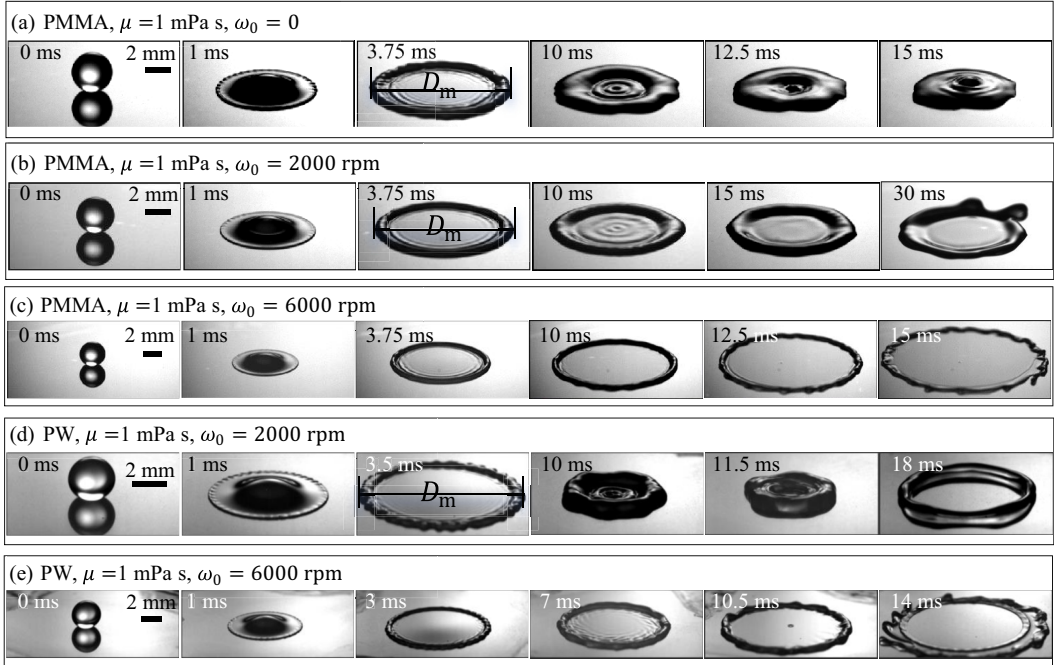


FIG. 2. Series of representative snapshots showing the typical behaviors of the impacting water droplets on polymethylmethacrylate (PMMA) or paraffin wax (PW) with different rotating speed ω_0 with the same impacting velocity 2.0 m s^{-1} : (a) PMMA surface with $\omega_0 = 0$, (b) PMMA surface with $\omega_0 = 2000 \text{ rpm}$, (c) PMMA surface with $\omega_0 = 6000 \text{ rpm}$, (d) PW surface with $\omega_0 = 2000 \text{ rpm}$, and (e) PW surface with $\omega_0 = 6000 \text{ rpm}$. The impacting behaviors are similar on surfaces with different wettabilities. After spreading to the maximum spreading diameter D_m , the droplet either deposits on the surface (a), or retracts to a certain radius (b) and (d). High surface rotating speed induces constant spreading of the droplet until its breakup (c) and (e).

film occurs at the front of the advancing lamella, which could be the result of centrifugal force induced by the rotating surface. We denote this sustained spreading of the droplet as *spreading breakup* in this study. For a droplet impacting on a hydrophobic surface, we also observe the emergence of the spreading retraction [Fig. 2(d)] and spreading breakup [Fig. 2(e)]. The transition of the droplet's impacting behavior from spreading retraction to spreading breakup is found to occur with sufficiently high ω_0 for impacting all the tested combinations of liquids and surfaces. For the droplet of the water-glycerol mixture, we observe similar impacting behaviors and transitions for all tested liquids.

In Fig. 3, we present the spreading curves, i.e., the spreading factor $\beta = D/D_0$ versus impact time t , for the water droplet impacting on four tested surfaces with different rotating speed ω_0 of the surface at the same impacting velocity $V_0 = 1.0 \text{ m s}^{-1}$. We observe an insignificant difference between the spreading curves in the early stage of spreading, i.e., right after the impact and before the droplet reaching the maximum spreading diameter ($t = t_c$). With the expanding of the ejected lamella, the spreading velocity gradually decreases, following the amplified differences between the spreading curves. We observe the noticeable deviations between the spreading curves at $t = t_c$, especially for the impact on the hydrophobic surface [Fig. 3(d)], and the enlarged distance between the spreading curves when $t > t_c$. The change in the spreading curves reflects the transition of the impacting behavior from spreading to spreading retraction and to spreading breakup with the increase of the surface's rotating speed.

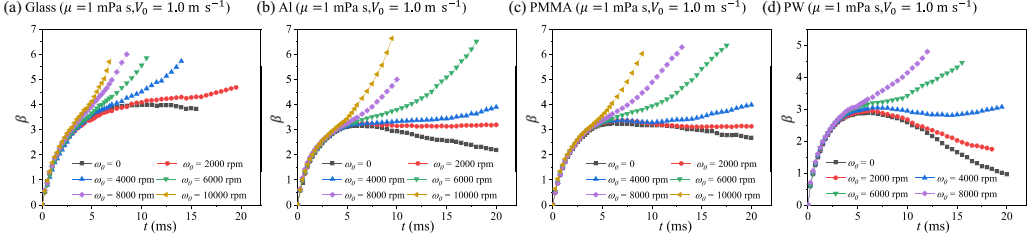


FIG. 3. The dependence of spreading factor $\beta = D/D_0$ on the time t for water droplets impacting on different rotating surfaces, including glass (a), Al (b), PMMA (c), and PW (d). The impacting velocity V_0 is kept at 1.0 m s^{-1} , while the rotating speed ω_0 of the surface ranges from 0 to 10 000 rpm.

For an impacting droplet targeted right at the center of a rotating surface, upon contact, the tangential shear force is spontaneously generated from the rotating surface due to the tangential velocity difference $\omega_0 R$ between the surface and the radial expanding lamella. The velocity difference between the rotating surface and the droplet increases with the expanding radius $R = D/2$, resulting in an increasing effect of tangential shear force on the tangential velocity building up in the advancing lamella. Such tangential velocity generates a centrifugal force, which locally accelerates the spreading of the droplet, resulting in the enhanced spreading or transition of the spreading behavior from spreading retraction to spreading breakup.

B. Enhanced spreading on rotating surface

We now focus on the spreading dynamic in the regimes of deposition and spreading retraction, in which the maximum spreading factor can be extracted from the spreading curve. We measure the maximum spreading factor $\beta_m = D_m/D_0$ from the spreading curve for impact on all tested surfaces. Besides the increase of β_m with the impacting Weber number We , we observe the gradual increase of β_m with the rotating speed ω_0 of the surface at the same We for all tested combinations of surfaces and liquids (Fig. 4). Therefore, the enhancement of spreading generally occurs on surfaces with various wettabilities.

To further reveal the enhancement effect of the rotating surface on the spreading dynamic, we first revisit the spreading dynamic of the droplet for impacting on a static flat surface. In the initial stage of the impact, shortly after the droplet contacts the surface, a thin liquid film, or lamella, is ejected from the bottom of the droplet with a typical initial high velocity and small thickness. This lamella expands radially with a decreasing radial velocity and increasing thickness until reaching the maximum spreading diameter or the emergence of splash. For the impact on a rotating surface, the tangential velocity of the expanding lamella is gradually built up by the tangential shear force that is associated with the radial position of the liquid. The generated tangential velocity induces the centrifugal force, accelerating the spreading of the expanding lamella and resulting in the enhancement of the maximum spreading factor. The increase of the radial expanding velocity V_r induced by the rotating surface tops up the radial spreading velocity determined by the initial impacting velocity V_0 . Therefore, the rotating surface enhances the spreading via the increase in kinetic energy.

To predict the enhancement effect of the rotating surface on the spreading droplet, the tangential velocity in the lamella needs to be firstly derived to calculate the radial acceleration caused by the centrifugal force. Considering a control volume of liquid, following the expanding characteristics of the generated lamella, the velocity and thickness of the expanding lamella changes with time. In addition, the tangential shear force from the rotating surface on the control volume relates with radial position. Therefore, the acting force and the mass of the control liquid volume both change with time, resulting in a complex acceleration process for tangential velocity of the lamella in the spreading stage.

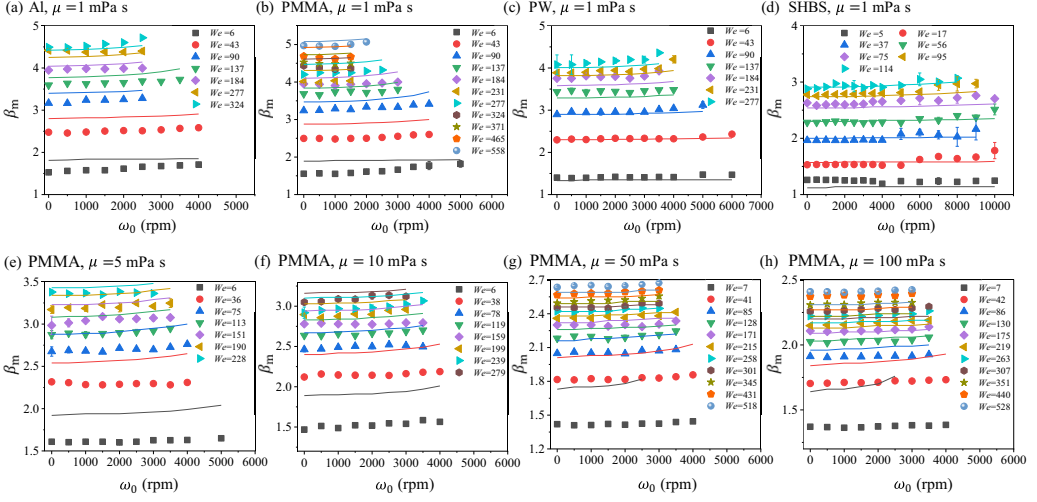


FIG. 4. Dependence of the maximum spreading factor β_m on the surface rotating speed ω_0 for impacting with various Weber numbers for different combinations of surfaces and liquids, including glass-water (a), PMMA-water (b), PW-water (c), SHBS-water (d), PMMA-water-glycerol mixture with $\mu = 5$ mPa s (e), PMMA-water-glycerol mixture with $\mu = 10$ mPa s (f), PMMA-water-glycerol mixture with $\mu = 50$ mPa s (g), and PMMA-water-glycerol mixture with $\mu = 100$ mPa s (h). The solid curves represent the theoretical predictions of the maximum spreading factor from our model.

To obtain a quantitative model to predict the enhancement effect of the rotating surface on the spreading dynamic, we adopt a simplified approach in the prediction of the built up tangential velocity V_θ , the key in spreading enhancement. We assume that the complex acceleration of tangential velocity V_θ in the advancing lamella can be approximated by a simplified acceleration process, in which the time to ejection and time-dependent thickness of the lamella is neglected. We consider the acceleration process of V_θ as an infinitesimal controlled volume $d\Omega$ of liquid with constant thickness h , moves with the same radial velocity $V = (\sqrt{3}/2)V_0\tau^{-1/2}$ as the expanding velocity of the lamella [8], from the impacting center, where $r = 0$ at $t = 0$, to the maximum spreading radius, where $r = D_m/2$ at $t = t_c$ [inset in Fig. 1(a)]. Here, $\tau = tV_0/R_0$ is the dimensionless time, and h is the thickness of the lamella when $r = D_m/2$ and $t = t_c$. During the spreading stage $0 < t \leq t_c$, the tangential velocity V_θ and radial velocity V_r of this controlled liquid volume are accelerated by the tangential shear force and centrifugal force, respectively. The increased radial velocity enhances the spreading, while the built-up tangential velocity generates a centrifugal force that may destabilize the liquid film at $t = t_c$, triggering the destabilization of the advancing lamella, i.e., the emergence of the spreading breakup.

For the infinitesimal controlled volume of the liquid, its mass dm is written as $dm = \rho hr dr d\theta$ in a cylindrical coordinate. Here, θ is the tangential coordinate. By applying linear approximation, the shear stress γ between the droplet and the rotating surface becomes $\gamma = \mu\omega_0 r/\delta$. Here, $\delta = R_0(\tau_c/Re)^{1/2}$ is the boundary layer thickness in the lamella. Here, $\tau_c = t_c/(R_0/V_0)$ is the dimensionless spreading time. The tangential shear force $dF_\gamma = \gamma r dr d\theta$ acting on the infinitesimal liquid body gives a tangential acceleration $a_\theta = dF_\gamma/dm = (\mu\omega_0 r)/(\delta\rho h)$. Therefore, the acceleration a_θ only relates with the radial position $r(t)$, which is assumed to have the same expanding characteristic as the front of the advancing lamella, i.e., $r = (3\tau)^{1/2}R_0$ [8]. Therefore, the tangential acceleration a_θ is the function of time t . Integrating the tangential acceleration a_θ from the moment of impact $t = 0$ to one moment t during the spreading, gives the tangential velocity in the advancing front of

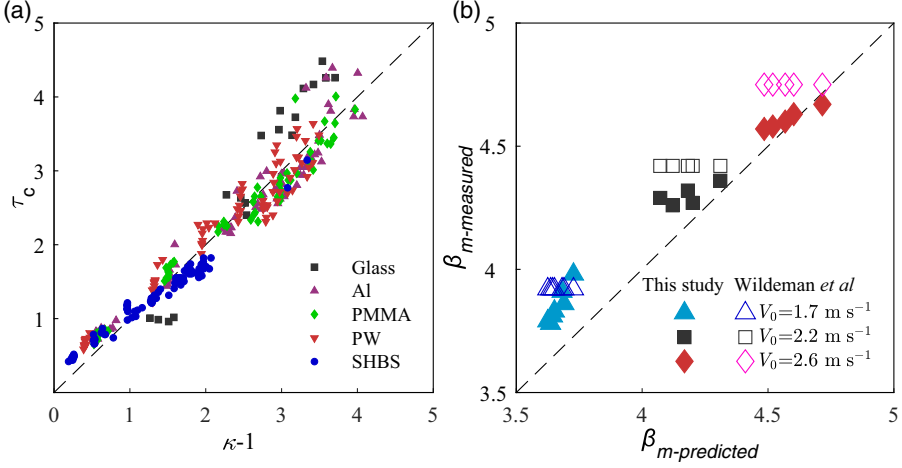


FIG. 5. (a) Comparison between the dimensionless spreading time τ_c and the dimensionless expression $\kappa - 1$ for all tested impacting cases in this study. (b) Comparison between the measured value of the maximum spreading factor $\beta_{m\text{-measured}}$ and the predicted ones $\beta_{m\text{-predicted}}$ from the model proposed in this study or Ref. [24] at three representative impacting velocities V_0 but with different rotating speed ω_0 on the PW surface. For the impact with $V_0 = 1.7 \text{ m s}^{-1}$, the rotating speed of the surface changes between 500 and 3500 rpm. For the impact with $V_0 = 2.2$ and 2.6 m s^{-1} , the rotating speed of the surface changes between 500 and 2500 rpm. The fitting parameter ϕ is set to 0.7 in the model proposed in Ref. [24], while it is changed to 0.8 in our model.

the lamella:

$$V_\theta(t) = \frac{2\mu\omega_0 R_0}{3\delta\rho h} \left(\frac{3V_0}{R_0} \right)^{1/2} t^{3/2}. \quad (1)$$

This built-up tangential velocity $V_\theta(t)$ induces the centrifugal force that generates a radial acceleration $a_r = V_\theta^2/r$ to facilitate the spreading. The integration of a_r with time t , gives the increased radial velocity $V_r(t)$ by the centrifugal force, expressed as

$$V_r(t) = \frac{6}{7} \left(\frac{2\mu\omega_0 R_0}{3\delta\rho h} \right)^2 \left(\frac{V_0}{3R_0^3} \right)^{1/2} t^{7/2}. \quad (2)$$

Therefore, as long as the spreading time t_c is determined, we can have the top-up radial velocity $V_r(t_c)$ of the spreading droplet caused by the rotating surface. Since the averaged spreading velocity is scaled with the impacting velocity V_0 , the increased spreading could be equivalent to the spreading with an increased velocity $V_0 + V_r(t_c)$. We are now ready to formulate the equation to predict the maximum spreading factor for an impacting droplet on a rotating surface. Here, we follow the energy conservation approach proposed by Wildeman *et al.* [24]. Based on the energy conservation, the sum of the initial surface energy $E_{s,0} = \pi D_0^2 \sigma$ and one-half of the initial kinetic energy $E_{k,0} = (\pi/12)\rho D_0^3 V_0^2$ is transferred to the combination of the final surface energy $E_s = (\pi/4)\sigma D_m^2 [1 - \cos(\alpha_\theta)] + \pi D_m h \sigma$ and viscous dissipation $E_d = \phi(V_0/\delta)^2 (D_m \delta t_c)$ in the boundary layer. Here, ϕ is a fitting parameter, and the dimensionless spreading time τ_c was found to be related with D_m/D_0 as $\tau_c = D_m/D_0 - 1 = \kappa - 1$ [24]. The lost one-half of the kinetic energy was considered to be dissipated by the head loss of impact. Although all these results were theoretically derived and experimentally confirmed for spreading a droplet on the static surface, we assume, in principle, they are still valid for droplet impact on rotating surfaces. We, indeed, find the dimensionless spreading time τ_c of the impacting droplet on the rotating surface is also related with D_m/D_0 as $\tau_c = D_m/D_0 - 1 = \kappa - 1$ [Fig. 5(a)].

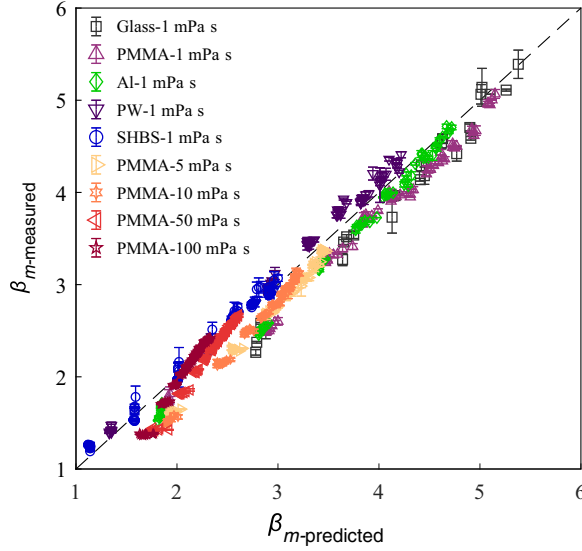


FIG. 6. Comparison between the measured value of the maximum spreading factor $\beta_{m\text{-measured}}$ and the predicted ones $\beta_{m\text{-predicted}}$ from the model proposed in this study for all impacting cases in the spreading regime.

The only difference lies in the kinetic energy E_{k0} . For impacting on a rotating surface, the radial advancing lamella is accelerated by the centrifugal force originating from the rotating surface. In other words, the extra kinetic energy is added into the spreading droplet on the rotating surface. To properly estimate the increased kinetic energy, we add the top-up of radial velocity $V_r(t = t_c)$ from Eq. (2) to the droplet's impacting velocity V_0 to provide an estimated kinetic energy $E_{r0} = (\pi/12)\rho D_0^3 V_{r0}^2$ during the impact caused by the rotating surface. Here, $V_{r0} = V_0 + V_r(t = t_c)$. Therefore, following the energy conservation approach, we have the equation connecting the total energy of the droplet before and after impact on the rotating surface:

$$E_{r0}/2 + E_{s0} = E_s + E_d. \quad (3)$$

By substituting the expressions of all the terms in Eq. (3) with the initial condition of the impact, it becomes an equation that can be numerically resolved for D_m . To a better fitting between the predicted values and measured ones, we revise the fitting parameter ϕ from its original value of 0.7 to 0.8, which could result from the additional dissipation caused by the rotating surface. In Fig. 5(b), we present the comparison between the measured maximum spreading factor $\beta_{m\text{-measured}}$ and the predicted ones $\beta_{m\text{-predicted}}$ from the model proposed in this study and Wildeman *et al.* [24] at three representative V_0 but with different ω_0 . It has to be noted that ϕ is set to 0.7 in the calculation of the predicted values using Wildeman's model, while it is changed to 0.8 in our model. The deviation between the predicted values calculated using these two models changes with the rotating speed ω_0 of the surface at the same V_0 , showing the enhancement effect of surface motion on β_m can be predicted by the proposed model in this study. We also plot $\beta_{m\text{-predicted}}$ versus $\beta_{m\text{-measured}}$ for impacting on all tested surfaces with different rotating speed ω_0 and impacting velocity V_0 in Fig. 6. Good agreement between the measured values and the predicted ones for all tested surfaces, suggesting the enhanced spreading induced by the rotating surface is well captured by the proposed model. It has to be noted that our model may not be applicable for the impacting with small Weber number and high rotating speed at high viscosity (the impacts with $We=7$ and $\omega_0 \geq 3000$ rpm for the droplet with $\mu \geq 50$ mPa s).

We observe the overprediction of the maximum spreading factor for impacting on the hydrophilic surfaces in Fig. 6. This overprediction could result from the underestimation of the advancing

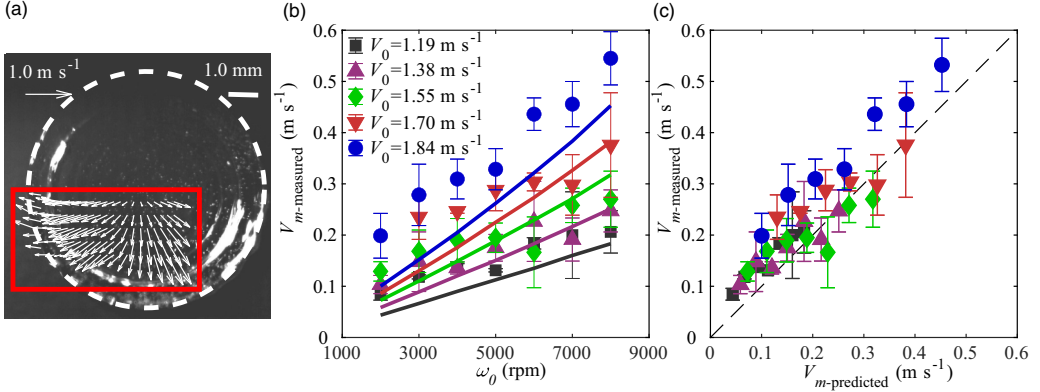


FIG. 7. (a) A representative flow field result for an impacting droplet with $V_0 = 1.54 \text{ m s}^{-1}$ on a rotating superhydrophobic surface with $\omega_0 = 5000 \text{ rpm}$. The red rectangle is the region where the flow field is measured. The dashed circle is the outer profile of the spreading droplet. (b) Dependence of the measured rotating velocity $V_{m\text{-measured}}$ around $t = t_c$ on the rotating velocity of the surface ω_0 for impacting on a superhydrophobic surface with different velocity V_0 . The solid curves represent the theoretical predictions of V_m . (c) The comparison between the measured rotating velocity $V_{m\text{-measured}}$ at $t = t_c$ and the predicted ones $V_{m\text{-predicted}}$ for impacting cases with different impact velocity V_0 and the surface's rotating speed ω_0 .

contact angle during the spreading. It has been reported that the advancing contact angle of the impacting droplet depends on both the surface's wettability and the flow field of the spreading droplet [42]. At high velocity, the advancing contact angle is reaching 180° as the surface wettability plays a minor role [24]. For the impacting droplet on a rotating surface, the flow field in the advancing lamella is modified by the rotating surface. Therefore, the measured advancing contact angle from the static surface, which is the advancing contact angle used in our model, may not be the same as those on a rotating surface. For the underprediction of the maximum spreading factor in Fig. 6, it could result from the modification of the fitting parameter accounting for the viscous dissipation.

C. The transition between spreading retraction and spreading breakup

For droplet impacting on a rotating surface, increasing the rotating speed ω_0 induces a higher centrifugal force $F_g \sim \rho V_\theta^2 / (D_m/2)$ at $t = t_c$, which eventually triggers the transition of the droplet's behavior from spreading retraction to spreading breakup. In this study, we first consider the transition between spreading retraction and spreading breakup for a water droplet, for which the viscous force can be neglected.

To predict such transition, we first calculate the tangential velocity $V_m = V_\theta(t = t_c)$ at $t = t_c$. According to the determined spreading time t_c , we are able to calculate the tangential velocity $V_{m\text{-predicted}}$ for all the impacting cases on rotating surfaces according to Eq. (1). To validate our calculation of V_m , we measured the tangential velocity $V_{m\text{-measured}}$ in the advancing lamella around the end of the spreading stage by particle image velocimetry [Fig. 7(c)]. In the experiment, we track the spreading diameter of the droplet to determine t_c , and obtain the correspondingly tangential velocity $V_{m\text{-measured}}$ [Fig. 7(a)]. We present the comparison between the measured value $V_{m\text{-measured}}$ and the predicted ones $V_{m\text{-predicted}}$ in Fig. 7(b). The data points scatter around the dashed line, where $V_{m\text{-measured}} = V_{m\text{-predicted}}$, validating our model in predicting the spreading dynamics for droplet impacting on the rotating surface.

We are now able to formulate the critical condition for the transition from spreading retraction to spreading breakup. For the centrifugal acceleration at $t = t_c$, it becomes $a_g \sim V_m^2 / (D_m/2)$, while the retracting acceleration caused by the capillary force can be written as $a_c \sim \sigma [1 - \cos(\alpha_a)] / (\rho r_1 r_2)$. Here, $r_1 = h/2 / \sin(\alpha_a/2)$ [43] and $r_2 = D_m/2$ are the radii of the curvature of lamella in two

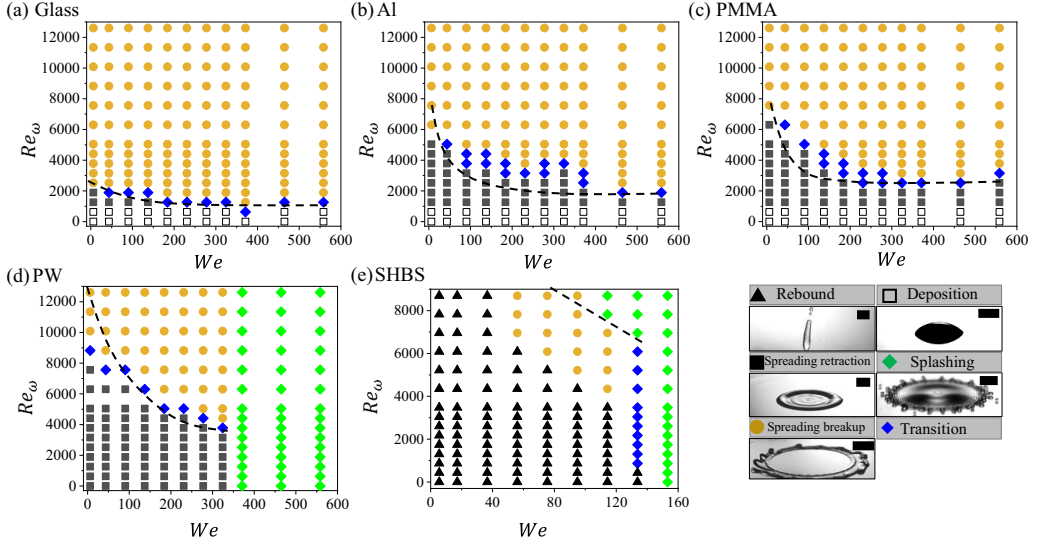


FIG. 8. Phase diagrams for the water droplet impacting behavior in the parameter space of rotational Reynolds number Re_ω and Weber number on different surfaces, including glass (a), PW (b), PMMA (c), PW (d), and SHBS (e). The dashed lines are the predicted transition from spreading retraction to spreading breakup. The scale bars represent 1 mm. Different behaviors of the impacting droplet are denoted with different markers. The behavior “transition” represents the state when the droplet’s behavior cannot be clearly classified.

directions. At the critical condition, a_g balances with a_c , i.e., $a_c \approx a_g$. Substituting the expressions above, gives the critical tangential velocity V_c at the transition:

$$V_c \sim \left(\frac{\sigma [1 - \cos(\alpha_a)] \sin(\alpha_a/2)}{\rho h} \right)^{1/2}. \quad (4)$$

Therefore, V_c depends on the wettability of the surface and the thickness of the lamella at $t = t_c$. For the spreading droplet on a rotating surface, the droplet would keep spreading until the liquid film breaks up when $V_m > V_c$, while the droplet may retract under the capillary force when $V_m \leq V_c$. At the same impacting velocity V_0 , the increase in ω_0 results in significant strengthening of V_θ as $V_\theta \propto \omega_0$, while slightly increasing in V_c since $V_c \propto h^{-1/2} \propto D_m$. Therefore, the increase in rotating speed ω_0 eventually leads to the emergence of spreading breakup.

We first conclude the impact behaviors of the water droplet on the tested surfaces, by presenting the phase diagrams of the droplet impacting behaviors on three surfaces in the parameter space of Re_ω versus We (Fig. 8). For the hydrophilic surfaces, the impacting behavior changes from deposition to spreading retraction to spreading breakup, with the increase of the rotating speed ω_0 of the surface. When $\omega_0 \leq 1000$ rpm, the droplet could stay on the rotating surface after spreading. At high rotating speed, i.e., $\omega_0 > 1000$ rpm, the droplet either retracts after reaching the maximum spreading diameter (spreading retraction) or keeps spreading until the liquid film destabilizes (spreading breakup). The transition between the spreading retraction to spreading breakup varies with both We and Re_ω . In general, the transition occurs at smaller Re_ω with the increase of We . This could be caused by the strengthened centrifugal force as the droplet spreads to a larger diameter. For the impacting on the hydrophobic surfaces, we observe the emergence of splashing at high We , and the disappearance of deposition at low Re_ω . For the impact targeted at the center of the rotating surface, the tangential shear force from the surface generates a rotating velocity in the spreading lamella, inducing a centrifugal force that is capable of facilitating the spreading or changing of the impacting behavior of the droplet.

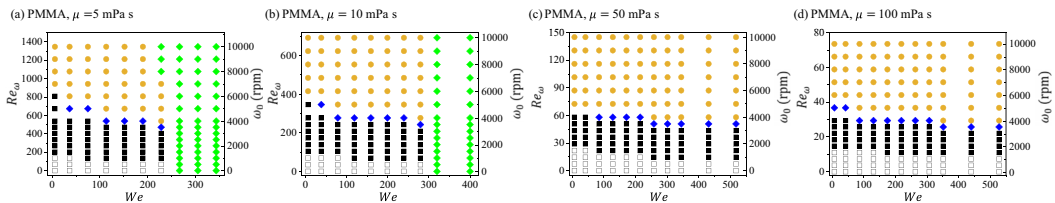


FIG. 9. Phase diagrams for impacting behavior in the parameter space of rotational Reynolds number and Weber number for the droplet of water/glycerol mixture with different viscosities, $\mu = 5$ mPa s (a), $\mu = 10$ mPa s (b), $\mu = 50$ mPa s (c) and $\mu = 100$ mPa s (d) on the PMMA surface.

We are now able to predict the critical tangential velocity V_c of the droplet at the transition between spreading retraction and spreading breakup at given impacting velocity V_0 . By increasing the rotating velocity of the surface, the tangential velocity V_m of the droplet at maximum spreading state ($D = D_m$) approaches and overwhelms the critical velocity V_c , i.e., $V_m \geq V_c$, triggering the transition of droplet behavior from spreading retraction to spreading breakup. However, from the experiment observation, the expanding lamella accumulates at the front, showing a fingering behavior that advances the transition [Figs. 2(c) and 2(e)]. Therefore, $V_m = nV_c$ could be more proper in determining the critical condition of the transition from spreading retraction to spreading breakup. Here, n is a fitting parameter. In this study, we take $n = 1/3$ and predict the transition between the two behaviors for a water droplet on all tested surfaces. The predicted transitions generally match well with the experimental observation (Fig. 8), validating our proposed model in predicting the critical condition for triggering the destabilization of the expanding liquid film on the rotating surface.

To present the effect of viscosity on the transition from spreading retraction to spreading breakup, we show the phase diagrams for impacting behavior in the parameter space of the rotational Reynolds number Re_{ω} and the Weber number for the droplet of water-glycerol mixture with different viscosities in Fig. 9. With the increase of liquid viscosity, the transition characteristics from spreading retraction to spreading breakup for high viscosity droplets deviates from those for water droplets. For the impact with water droplets on a PMMA surface, the transition from spreading retraction to spreading breakup depends on both the Weber number and the rotational Reynolds number. The critical rotational Reynolds number at the transition generally decreases with the Weber number [Fig. 8(c)]. However, for the impact with high viscosity, we observe the decreasing effect of the impacting Weber number on the transition, especially for the impacts with $\mu = 50$ mPa s and $\mu = 100$ mPa s. Although the critical rotational Reynolds number varies for impact with different viscosities, the transition typically occurs when the rotating speed is around 4000 rpm. This could result from the competition between the centrifugal force and the viscous force, both of which increase with liquid viscosity. The former one promotes the transition, while the latter one resists the transition. However, the viscous effect is neglected in our prediction of the transition. To predict the transition from spreading retraction to spreading breakup for the droplet with high viscosity, further work has to consider the effect of the viscous force.

IV. CONCLUSIONS

In this study, we present a detailed study in characterizing and analyzing the behaviors of the droplets impacting right on the center of rotating surfaces with various combinations of surfaces and liquids. We observe the droplet's impacting behavior changes from deposition to spreading retraction to spreading breakup, with the increase of the surface's rotating speed. The tangential shear force from the rotating surface induces a tangential velocity that either enhances the spreading or further destabilizes the expanding lamella. We derived the increased tangential velocity in the impacting droplet by adopting a simplified approach and validated the predicted tangential velocity

by particle image velocimetry measurement. We further deduced an equation based on energy conservation to quantitatively describe the enhanced maximum spreading factor in the spreading regime for all tested combinations of surfaces and liquids, and derived the critical condition for the transition from spreading retraction to spreading breakup for water droplets on surfaces with various wettabilities. The predicted values generally match well with the measured ones for all tested surfaces with various wettabilities for water droplets, suggesting the potential of our proposed models in the prediction of the droplet's spreading dynamics and manipulation of the droplet's behavior in the complex droplet-interface interaction.

ACKNOWLEDGMENTS

We would like to acknowledge the support from the National Natural Science Foundation of China (Grant No. 12302324) and National Science and Technology Major Project (Grant No. 2022-III-0003-0012).

-
- [1] S. Lin, B. Zhao, S. Zou, J. Guo, Z. Wei, and L. Chen, Impact of viscous droplets on different wettable surfaces: Impact phenomena, the maximum spreading factor, spreading time and post-impact oscillation, *J. Colloid Interface Sci.* **516**, 86 (2018).
 - [2] D. Quéré, Leidenfrost dynamics, *Annu. Rev. Fluid Mech.* **45**, 197 (2013).
 - [3] C. Josserand and S. T. Thoroddsen, Drop impact on a solid surface, *Annu. Rev. Fluid Mech.* **48**, 365 (2016).
 - [4] X. Peng, T. Wang, F. Jia, K. Sun, Z. Li, and Z. Che, Singular jets during droplet impact on superhydrophobic surfaces, *J. Colloid Interface Sci.* **651**, 870 (2023).
 - [5] Z. Hu, X. Zhang, S. Gao, Z. Yuan, Y. Lin, F. Chu, and X. Wu, Axial spreading of droplet impact on ridged superhydrophobic surfaces, *J. Colloid Interface Sci.* **599**, 130 (2021).
 - [6] B. Zhang, V. Sanjay, S. Shi, Y. Zhao, C. Lv, X.-Q. Feng, and D. Lohse, Impact forces of water drops falling on superhydrophobic surfaces, *Phys. Rev. Lett.* **129**, 104501 (2022).
 - [7] M.-J. Thoraval, K. Takehara, T. G. Etoh, S. Popinet, P. Ray, C. Josserand, S. Zaleski, and S. T. Thoroddsen, von Kármán vortex street within an impacting drop, *Phys. Rev. Lett.* **108**, 264506 (2012).
 - [8] G. Riboux and J. M. Gordillo, Experiments of drops impacting a smooth solid surface: A model of the critical impact speed for drop splashing, *Phys. Rev. Lett.* **113**, 024507 (2014).
 - [9] Y. Aksoy, P. Eneren, E. Koos, and M. Vetrano, Spreading-splashing transition of nanofluid droplets on a smooth flat surface, *J. Colloid Interface Sci.* **606**, 434 (2022).
 - [10] D. Bartolo, A. Boudaoud, G. Narcy, and D. Bonn, Dynamics of non-Newtonian droplets, *Phys. Rev. Lett.* **99**, 174502 (2007).
 - [11] M.I. Smith and V. Bertola, Effect of polymer additives on the wetting of impacting droplets, *Phys. Rev. Lett.* **104**, 154502 (2010).
 - [12] J. C. Fernández-Toledano, B. Braeckveldt, M. Marengo, and J. De Coninck, How wettability controls nanoprinting, *Phys. Rev. Lett.* **124**, 224503 (2020).
 - [13] J. M. Gordillo, G. Riboux, and E. S. Quintero, A theory on the spreading of impacting droplets, *J. Fluid Mech.* **866**, 298 (2019).
 - [14] H. Almohammadi and A. Amirfazli, Droplet impact: Viscosity and wettability effects on splashing, *J. Colloid Interface Sci.* **553**, 22 (2019).
 - [15] L. Xia, Z. Yang, F. Chen, T. Liu, Y. Tian, and D. Zhang, Droplet impacting on pillared hydrophobic surfaces with different solid fractions, *J. Colloid Interface Sci.* **658**, 61 (2024).
 - [16] T. C. Sykes, B. D. Fudge, M. A. Quetzeri-Santiago, J. R. Castrejón-Pita, and A. A. Castrejón-Pita, Droplet splashing on curved substrates, *J. Colloid Interface Sci.* **615**, 227 (2022).
 - [17] A. U. Siddique, M. Trimble, F. Zhao, M. M. Weislogel, and H. Tan, Jet ejection following drop impact on micropillared hydrophilic substrates, *Phys. Rev. Fluids* **5**, 063606 (2020).

- [18] J. Lee, N. Laan, K. G. de Bruin, G. Skantzaris, N. Shahidzadeh, D. Derome, J. Carmeliet, and D. Bonn, Universal rescaling of drop impact on smooth and rough surfaces, *J. Fluid Mech.* **786**, R4 (2016).
- [19] Z. Jian, C. Josserand, S. Popinet, P. Ray, and S. Zaleski, Two mechanisms of droplet splashing on a solid substrate, *J. Fluid Mech.* **835**, 1065 (2018).
- [20] L. Xu, W. W. Zhang, and S. R. Nagel, Drop splashing on a dry smooth surface, *Phys. Rev. Lett.* **94**, 184505 (2005).
- [21] J. Hao, J. Lu, L. Lee, Z. Wu, G. Hu, and J.M. Floryan, Droplet splashing on an inclined surface, *Phys. Rev. Lett.* **122**, 054501 (2019).
- [22] E. Q. Li, K. R. Langley, Y. S. Tian, P. D. Hicks, and S. T. Thoroddsen, Double contact during drop impact on a solid under reduced air pressure, *Phys. Rev. Lett.* **119**, 214502 (2017).
- [23] D. A. Burzynski, I. V. Roisman, and S. E. Bansmer, On the splashing of high-speed drops impacting a dry surface, *J. Fluid Mech.* **892**, A2 (2020).
- [24] S. Wildeman, C. W. Visser, C. Sun, and D. Lohse, On the spreading of impacting drops, *J. Fluid Mech.* **805**, 636 (2016).
- [25] N. Laan, K. G. de Bruin, D. Bartolo, C. Josserand, and D. Bonn, Maximum diameter of impacting liquid droplets, *Phys. Rev. Appl.* **2**, 044018 (2014).
- [26] C. Clanet, C. Béguin, D. Richard, and D. Quéré, Maximal deformation of an impacting drop, *J. Fluid Mech.* **517**, 199 (2004).
- [27] N. Satpathi, K. Nampoothiri, and A. Sen, Effects of surface acoustic waves on droplet impact dynamics, *J. Colloid Interface Sci.* **641**, 499 (2023).
- [28] X. Zhang, Z. Zhu, C. Zhang, and C. Yang, Reduced contact time of a droplet impacting on a moving superhydrophobic surface, *Appl. Phys. Lett.* **117**, 151602 (2020).
- [29] H. Zhan, C. Lu, C. Liu, Z. Wang, C. Lv, and Y. Liu, Horizontal motion of a superhydrophobic substrate affects the drop bouncing dynamics, *Phys. Rev. Lett.* **126**, 234503 (2021).
- [30] J.-X. Wang, J. Qian, J.-X. Li, X. Wang, C. Lei, S. Li, J. Li, M. Zhong, and Y. Mao, Enhanced interfacial boiling of impacting droplets upon vibratory surfaces, *J. Colloid Interface Sci.* **658**, 748 (2024).
- [31] M. Song, H. Zhao, T. Wang, S. Wang, J. Wan, X. Qin, and Z. Wang, A new scaling number reveals droplet dynamics on vibratory surfaces, *J. Colloid Interface Sci.* **608**, 2414 (2022).
- [32] Y. Liu, P. Tan, and L. Xu, Kelvin–Helmholtz instability in an ultrathin air film causes drop splashing on smooth surfaces, *Proc. Natl. Acad. Sci. USA* **112**, 3280 (2015).
- [33] M. Pegg, R. Purvis, and A. Korobkin, Droplet impact onto an elastic plate: A new mechanism for splashing, *J. Fluid Mech.* **839**, 561 (2018).
- [34] J. M. Gordillo and G. Riboux, A note on the aerodynamic splashing of droplets, *J. Fluid Mech.* **871**, R3 (2019).
- [35] T. de Goede, K. de Bruin, N. Shahidzadeh, and D. Bonn, Droplet splashing on rough surfaces, *Phys. Rev. Fluids* **6**, 043604 (2021).
- [36] H. Law and V. Koutsos, Leading edge erosion of wind turbines: Effect of solid airborne particles and rain on operational wind farms, *Wind Energy* **23**, 1955 (2020).
- [37] L. Li, Y. Liu, and H. Hu, An experimental study on dynamic ice accretion process over the surfaces of rotating aero-engine spinners, *Exp. Therm Fluid Sci.* **109**, 109879 (2019).
- [38] F. Chu, S. Li, Z. Hu, and X. Wu, Regulation of droplet impacting on superhydrophobic surfaces: Coupled effects of macrostructures, wettability patterns, and surface motion, *Appl. Phys. Lett.* **122**, 160503 (2023).
- [39] S. Moghtadernejad, M. Jadidi, Z. Johnson, T. Stolpe, and J. Hanson, Droplet impact dynamics on an aluminum spinning disk, *Phys. Fluids* **33**, 072103 (2021).
- [40] R. Tao, W. Fang, J. Wu, B. Dou, W. Xu, Z. Zheng, B. Li, Z. Wang, X. Feng, and C. Hao, Rotating surfaces promote the shedding of droplets, *Research* **6**, 0023 (2023).
- [41] F. Scarano, Tomographic PIV: Principles and practice, *Meas. Sci. Technol.* **24**, 012001 (2013).
- [42] Š. Šikalo, H.-D. Wilhelm, I. V. Roisman, S. Jakirlić, and C. Tropea, Dynamic contact angle of spreading droplets: Experiments and simulations, *Phys. Fluids* **17**, 062103 (2005).
- [43] P.-G. Gennes, F. Brochard-Wyart, and D. Quéré, *Capillarity and Wetting Phenomena: Drops, Bubbles, Pearls, Waves* (Springer, New York, 2004).